THE JOURNAL OF PHYSICAL CHEMISTRY C

Article

Cite This: J. Phys. Chem. C 2018, 122, 28351−28361

pubs.acs.org/JPCC

Insights into the Synthesis Mechanism of Ag_{29} Nanoclusters

Marte van der Linden,[†,‡] Arnoldus J. van Bunningen,[§] Mario U. Delgado-Jaime,[∥] Blanka Detlefs,[‡] Pieter Glatzel,[‡] Alessandro Longo,[⊥,#] and Frank M. F. de Groot*[,†]

[†]Inorganic Chemistry and Catalysis, Debye Institute for Nanomaterials Science, Utrecht University, Universiteitslaan 99, 3584 CG Utrecht, The Netherlands

[‡]European Synchrotron Radiation Facility, 71 Avenue des Martyrs, CS 40220, 38043 Grenoble, France

[§]Condensed Matter and Interfaces, Debye Institute for Nanomaterials Science, Utrecht University, Princetonplein 1, 3584 CC Utrecht, The Netherlands

[∥]Department of Chemistry, University of Guadalajara, Blvd. Marcelino Garcia Barragán 1421, 44430 Guadalajara, Mexico

[⊥]Netherlands Organization for Scientific Research at ESRF, BP 220, 38043 Grenoble Cedex 9, France

[#]Istituto per lo Studio dei Materiali Nanostrutturati (ISMN)-CNR, UOS Palermo, Via Ugo La Malfa 153, 90146 Palermo, Italy

Supporting Information

ABSTRACT: The current understanding of the synthesis mechanisms of noble metal clusters is limited, in particular for Ag clusters. Here, we present a detailed investigation into the synthesis process of atomically monodisperse Ag_{29} clusters, prepared via reduction of $AgNO_3$ in the presence of dithiolate ligands. Using optical spectroscopy, mass spectrometry, and X-ray spectroscopy, it was determined that the synthesis involves a rapid nucleation and growth to species with up to a few hundred Ag atoms. From these larger species, Ag_{29} clusters are formed and their concentration increases steadily over time. Oxygen plays an important role in the etching of large particles to Ag_{29}. No other stable Ag cluster species are observed at any point during the synthesis.

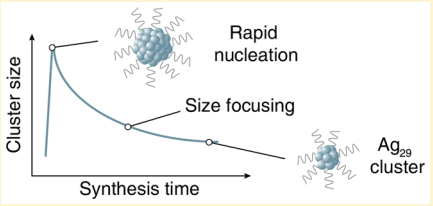

INTRODUCTION

Noble metal nanoclusters, with up to a few hundred atoms, have attracted widespread attention due to their small size and properties not found in larger nanoparticles, such as nonbulk structures, potentially atomic monodispersity, and luminescence.[1] These clusters may find applications in catalysis, sensing, and bioimaging.[2] Cluster properties are size-dependent, and with atomic monodispersity, it becomes possible to correlate properties with size at the single atom level. It is therefore of great interest to prepare atomically monodisperse clusters in bulk quantities and with high yields, preferably without resorting to multistep reactions or extensive purification protocols. To date, this has been achieved for a number of highly stable magic number gold and silver clusters, notably $Ag_{44}(SR)_{30}$ and $Au_{25}(SR)_{18}$, where SR indicates a thiolate ligand.[3−7] New synthesis protocols are constantly being developed and improved so that increasingly, also less stable sizes can be more easily obtained. For example, the cluster $Au_{18}(SR)_{14}$ was at first only prepared in a mixture with multiple different sizes and had to be isolated using gel electrophoresis.[8] More recently, a pH controlled reduction method was developed, which directly yielded the monodisperse cluster in high quantitites.[9] Knowledge of the mechanisms of cluster synthesis have made this progress possible.

Studies of cluster synthesis have focused on gold clusters and have determined a number of factors that can influence the product(s) obtained from a reaction. These include reaction temperature,[10] solvent[11−13] and even stirring speed.[14,15] At first glance this may seem like the development of a good synthesis protocol is more art than science. However, some general principles have been established. It is commonly accepted that the synthesis of clusters proceeds via a kinetically controlled reduction reaction.[16] The precursor for cluster synthesis is usually a simple metal salt such as $HAuCl_4$ which is mixed with thiols in solution. After formation of this synthesis intermediate, a reducing agent (often $NaBH_4$) is added to reduce metal ions. Nucleation occurs, followed by growth. A large number of different cluster and nanoparticle species may be formed. The solution is then aged to obtain the final product. This may involve a change in synthesis conditions such as a change of solvent and addition of a different ligand to etch clusters to the desired size.[11] During aging, thermodynamics becomes of greater importance. As some species are inherently less stable than others, they will convert to the more stable species, which are the final products of the reaction. This spontaneous process is called size focusing.[16−18] To obtain a different product, the initial size distribution of clusters can be changed. This can be done for example by changing the solvent, temperature or stirring speed. These parameters

Received: September 25, 2018
Revised: November 2, 2018
Published: November 19, 2018

DOI: 10.1021/acs.jpcc.8b09360
J. Phys. Chem. C 2018, 122, 28351−28361

influence the rate of the reduction, but also the extent of aggregation of the Au(I)-thiolate intermediate for Au clusters.[10]

Less is known about the synthesis mechanisms of Ag clusters. Therefore, in this article, we investigate the synthesis of silver nanoclusters capped with the dithiolate ligand lipoic acid (LA). We have previously characterized this cluster and found that its composition is $Ag_{29}(LA)_{12}^{3-}$.[19] Each LA binds bidentate, which makes it a magic number cluster with 8 electrons.[20] Most importantly, our previous work found that atomically monodisperse Ag_{29} can be obtained without any purification. Once the synthesis starts, there are no further changes to the reaction mixture. This makes it an ideal candidate for a detailed investigation. We prepare these clusters via a bottom-up approach using $AgNO_3$, but a top-down method involving etching of larger nanoparticles with excess LA also yields Ag_{29}.[21] It may be that similar size focusing mechanisms are occurring in both cases.

In this study, we investigate the formation of $Ag_{29}(LA)_{12}^{3-}$ from $AgNO_3$ using optical spectroscopy, mass spectrometry, and X-ray absorption spectroscopy (XAS). XAS was found to be an especially useful technique, as it is element specific and does not require extensive sample purification which may affect the compositions of the clusters. From XAS, one can obtain information about the electronic structure and local geometry of the absorber.[22−24] A XAS spectrum is usually divided in two regions: the extended X-ray absorption fine structure (EXAFS) and X-ray absorption near edge structure (XANES). Quantitative information about bond lengths and coordination numbers can be obtained from EXAFS by fitting to the EXAFS equation.[22] Analysis of XANES is more complicated and requires comparison to spectra of reference compounds or calculations. Both techniques were used to study the formation of Ag_{29} clusters.

While the nucleation and initial growth could not be studied in detail, it was determined that, within minutes of reduction, large clusters or nanoparticles with a hundred or more Ag atoms are present. Size focusing to Ag_{29} then occurs, possibly via Ag_{28} and Ag_{26}, and the remarkable stability of Ag_{29} clusters is an important factor in their successful synthesis. The conversion of $Ag_{\sim 100}$ to Ag_{29} likely proceeds via an etching mechanism where oxygen plays an important role.

METHODS

Chemicals. $AgNO_3$ was obtained from Fisher Scientific (laboratory reagent grade) or Sigma-Aldrich (≥99.0%). $NaBH_4$ (99%), (±)-α-lipoic acid (≥99%), methanol (≥99.9%), Ag powder (≥99.9%), Ag_2O (99%), Ag_2S (99.9%), and silver diethyldithiocarbamate (99%) were purchased from Sigma-Aldrich. 1-Butanol (99.5%) was obtained from Acros. Water was of Milli-Q quality, purified using a Millipore Direct-Q 3 water purification system.

Synthesis. The synthesis of the Ag clusters is adapted from that of Adhikari et al.[25] and is the same as that used in our previous studies.[19,26] Full details are given in the Supporting Information. For X-ray spectroscopy experiments, the synthesis was scaled up 5× without any further modifications to the protocol. The pH of the cluster solution is ∼9.

Optical Spectroscopy. UV−vis spectra were recorded using a PerkinElmer Lambda 950 or a PerkinElmer Lambda 40. Emission spectra were recorded with a 450 W xenon lamp and a Spex 1680 (0.22m) spectrofluorometer for excitation and an Acton Research SpectraPro 300i monochromator with a liquid N_2 cooled Princeton Instruments CCD camera for detection of emission spectra. The CCD camera was equipped with a 150 lines/mm grating blazed at 800 nm. The excitation wavelength was 420 nm.

Mass Spectrometry. MS measurements were performed in negative ion mode using an electrospray ionization time-of-flight (ESI-ToF) instrument (LC-T; Micromass, Manchester, U.K.) equipped with a Z-spray nanoelectrospray ionization source. Needles were made from borosilicate glass capillaries (Kwik-Fil, World Precision Instruments, Sarasota, FL) on a P-97 puller (Sutter Instruments, Novato, CA), coated with a thin gold layer by using an Edwards Scancoat (Edwards Laboratories, Milpitas, CA) six Pirani 501 sputter coater. After purification, the sample was sprayed into the mass spectrometer. The applied voltage on the needle was 1180 V and the sample cone voltage was varied between −5 and 0 V. All spectra were mass calibrated in negative ion mode, using an aqueous solution of phosphoric acid (0.1% v/v). All samples were purified using 1-butanol (BuOH) to extract water, containing excess ligands and other possible contaminants, in several steps until the clusters sediment, after which they are washed with a small amount of methanol (MeOH) and redispersed in water. Full details are given in the Supporting Information.

EXAFS. Ag K-edge EXAFS (25.51 keV) was measured at BM26A (DUBBLE) of the European Synchrotron Radiation Facility.[27] The incident beam was selected using a Si(111) monochromator. The measurements were performed in fluorescence mode using an 8 element Ge detector. Samples were measured in capillaries (Hilgenberg, 2 mm outside diameter, article no. 4007620).

EXAFS was recorded of concentrated Ag cluster solution prepared a few days before the measurement. The clusters were concentrated around 5× using 3 kDa cutoff filters (Amicon, Millipore) and then typically measured for 30−60 min (4 scans). After this, a new sample was prepared and measured. This was done in order to avoid radiation damage. The final spectrum was averaged over 25 spectra taken from seven freshly concentrated aliquots of the same batch of clusters. EXAFS during synthesis was recorded by taking aliquots at regular intervals during synthesis. Each aliquot was measured for no more than 60 min. As the synthesis is ongoing, the sample compositions will change somewhat during this time, and this is the reason we did not measure for longer times. In combination with the low Ag concentration (1 mM), this means that the EXAFS data are rather noisy; above the edge, the counts per second are $1-2 \times 10^4$, compared to a background of 5×10^3 counts below the edge.

EXAFS analysis was done using VIPER,[28] and the Athena and Artemis[29] software packages. Scattering phases and amplitudes were calculated using FEFF for a number of different compounds, including Ag and Ag_2S, coordinates of which were obtained from the Inorganic Crystal Structure Database[30] (numbers 44387 and 44507, respectively), as well as $Ag_{29}(BDT)_{12}(TPP)_4$,[31] with TPP (triphenylphosphine) ligands removed and BDT (1,3-benzenedithiol) replaced by LA. To ensure reasonable C−C and C−H bond lengths and angles in the newly added LA ligands, the geometry of the ligands was optimized using molecular mechanics (UFF force field, steepest descent algorithm) in Avogadro.[32] The positions of Ag and S atoms were fixed so that the core structure remained unchanged.

DOI: 10.1021/acs.jpcc.8b09360
J. Phys. Chem. C 2018, 122, 28351−28361

One Ag−Ag and one Ag−S path were used in the fit. Typical fit parameters for as-synthesized clusters were: k = 3.0−12.5 Å^{-1}, R = 1.0−3.2 Å, using a Hanning window (dk = 1 Å^{-1}) for the Fourier transformation. Fitting was done using k = 3 weighting in VIPER and k = 1, 2, 3 weighting in Artemis. The compound from which the scattering path was calculated had a minor effect on the fit, as had the fitting software and parameters. Clusters during synthesis were measured over a shorter k-range, k = 3.0−8.15 Å^{-1}, and R = 1.0−3.45 Å. To determine coordination numbers during synthesis, a number of parameters were fixed to that of as-synthesized clusters, such as bond lengths or Debye−Waller factors, or both, of the two scattering paths.[33] A number of fits showed unreasonable parameters, such as negative Debye−Waller factors or extremely short bond lengths. These fits were discarded and excluded from further analysis. Regardless of whether none, two or four parameters were fixed in the fit, the results show similar trends. The amplitude reduction factor S_0^2 was not explicitly taken into account during fitting (i.e., S_0^2 = 1 was used). However, from fitting a reference Ag sample and assuming transferability, it may be estimated, S_0^2 = 0.9.

XANES. Ag L_3-edge XANES (3.35 keV) was recorded at beamline ID26 at the European Synchrotron Radiation Facility. The incident beam was selected using the (111) reflection from a double Si crystal monochromator. Higher harmonics were suppressed using a Si coated mirror at an angle of 3.5 mrad. The typical beam size on the sample was 500 × 100 μm^2 (H × V), with a photon flux of 1 × 10^{13} s^{-1}. X-ray fluorescence was collected at a 90° angle using a silicon drift detector (SDD). The detector signal was corrected for any nonlinearity (or saturation effects) at high count rates, and all spectra were normalized for incident photon flux.

For XANES, the Ag_{29} synthesis was done at 5× the normal scale to give a final sample volume of 83.5 mL, while all reagent concentrations were unchanged. The scaling up does not affect the synthesis process or the final sample composition.[19] The sample was placed in a vial from which liquid was pumped through a 1.5 mm capillary to form a free-standing liquid jet which was placed in the focus of the beam. Below the jet, the liquid was collected and returned to the synthesis vial. To avoid attenuation of X-rays through air, the jet was run through a chamber filled with helium. The chamber had a kapton window on one side for the incoming X-ray beam, and another where the detector was placed. Pumping and purging with He was required to avoid absorption by argon present in air (K-edge 3.21 keV). The slight overpressure of He in the chamber resulted in saturation of the Ag cluster solution with He, which we believe was beneficial in preventing radiation damage when studying as-synthesized clusters. Despite exposure to X-rays for 7 h, the change in UV−vis absorption spectra was minimal. This was in great contrast to what was seen when the same liquid jet setup, but without He chamber, was used in an attempt to record Ag K-edge EXAFS (25.51 keV). Then, the sample darkened noticeably and absorption features had all but disappeared after the same time, despite this experiment being carried out on a bending magnet beamline rather than an undulator beamline.

To monitor sample changes, we also recorded UV−vis absorption spectroscopy by pumping the solution through a Hellma 3-in-1 flow cuvette (product no. 176-766-15-40, 2 mm path length) which was built into the circuit just before the capillary. The excitation source was an Ocean Optics DH-2000-BAL lamp equipped with an Ocean Optics FVA-UV fiber optic variable attenuator, and transmitted light was detected using an Ocean Optics Maya 2000 Pro spectrometer. The attenuator was positioned between the lamp and flow cuvette to decrease the intensity of UV−vis light, which was necessary to avoid saturation of the spectrometer. By recording a blank and dark spectrum, the absorbance of the sample was immediately calculated by the software (SpectraSuite). A schematic figure of the setup is shown in Figure 1.

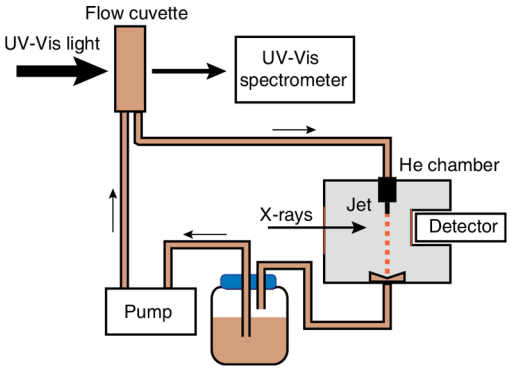

Figure 1. Liquid jet setup with continuous flow for recording X-ray absorption spectroscopy in a He atmosphere. The sample is pumped from the reservoir first through a flow cuvette to record UV−vis spectroscopy and then through a capillary nozzle to form a freestanding jet in a chamber with He, where X-ray spectroscopy can be measured. The detector is placed at a 90° angle to the incoming beam to collect fluorescence.

Reference compounds were measured as solids. They were mixed with boron nitride, using around 15 mg of compound for 40 mg of boron nitride for $AgNO_3$, Ag_2O, Ag and silver diethyldithiocarbamate. After mixing, the samples were spread thinly on kapton tape before being measured in a cryostat (KONTI, CryoVac) cooled with liquid He. The typical operating temperature was 40 K. Ag was prepared with different dilutions (10 mg mixed with 30, 80, and 110 mg boron nitride) to test for self-absorption. There was no difference between the spectra of these three dilutions. Sample preparation and measurement of Ag_2S was done by mixing 4 mg of the compound with 50 mg of cellulose and pressing it into a 13 mm diameter pellet. The spectrum was recorded at room temperature in the He chamber. No significant radiation damage was observed, but nevertheless as a precaution, multiple spots on each sample were measured. A solution of $AgNO_3$ (10 mM) was also measured in the liquid jet setup, although this solution proved susceptible to radiation damage.

The experimental spectrum of Ag_{29} clusters was compared to spectra of reference compounds, as well as spectra calculated using FDMNES.[34] The structure of the cluster was taken from that of Ag_{29} protected with BDT,[31] modified in the same way as for EXAFS. The FDMNES calculation was done of each of the 29 Ag atoms in the cluster, using a radius of 6 Å for each calculation. This corresponds to the distance from the central to the outermost Ag atoms. Atomic potentials, Fermi level, and charge transfer were calculated self-consistently and the finite difference method was used to calculate potentials.[35,36] Relativistic effects were taken into account. The spectrum was convoluted to apply an energy-dependent broadening, using default parameters (an arctangent function). The width of the core-hole was decreased slightly to 1.50 eV to better match the experimental data. Additional calculations were

DOI: 10.1021/acs.jpcc.8b09360
J. Phys. Chem. C 2018, 122, 28351−28361

performed using FEFF 9.6[37] for four different Ag atoms in the cluster; the central atom (1 site), one in the icosahedral shell (12 sites), one in an Ag_3S_6 crown (12 sites) and one external Ag atom (4 sites). The final spectrum was taken as the weighted average of these. Calculations were done using a screened (FSR) core-hole, Hedin-Lundquist exchange model, full multiple scattering (FMS, radius 6 Å) and self-consistently calculated potentials (SCF, radius 4 Å). For both FEFF and FDMNES calculations, only dipole transitions are considered ($\Delta l = \pm 1$). The individual contributions to the spectrum of d and s final states, $\Delta l = +1$ and -1, respectively, were also calculated with FDMNES, using the *lminus1* and *lplus1* commands.

RESULTS AND DISCUSSION

Synthesis of Ag_{29} Studied with Optical Spectroscopy. The synthesis process of Ag_{29} clusters involves the addition of $AgNO_3$ to an aqueous solution of LA and $NaBH_4$, the latter being added to deprotonate LA and reduce it to DHLA, thus making it water-soluble. This solution is pale yellow and turbid. Subsequently, more $NaBH_4$ was added to reduce the silver ions. Within minutes of this, the solution turned dark and then gradually lightened to bright, reddish orange. The final cluster solution shows strong red luminescence and characteristic absorption features at 330, 425, and 500 nm. These emission and absorption features have previously been shown to originate from Ag_{29} in solutions containing no other cluster sizes and can therefore be used to study the formation of the clusters.[19] In total, the synthesis process takes ~6 h, although there is some variation between samples.

Absorption and emission spectra of Ag clusters during synthesis were recorded by taking aliquots at regular intervals. Spectra are shown in Figure 2. The initial dark solution is not luminescent and shows only a broad absorption feature around 480 nm, which may indicate the presence of particles larger than 29 atoms, with a broad size distribution.[21,38−40] Luminescence appears after around 50 min, which coincides with the lightening of the sample and the emergence of the absorption features at 330, 425, and 500 nm. From the normalized luminescence spectra, it can be seen that the shape of the emission peak hardly changes after the first appearance. There is only a slight decrease in relative intensity of the near-infrared (NIR) luminescence. Possibly this NIR luminescence originates from clusters that are not fully protected by ligands (it was also observed for clusters with lower LA concentrations[19]). The Ag_{29} cluster is clearly present in low concentration in the first hour of the synthesis, and its concentration increases in time until virtually all Ag is present as Ag_{29}.

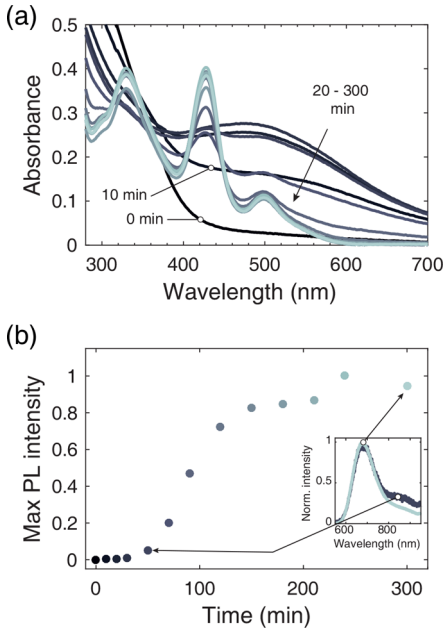

Figure 2. Optical properties of Ag_{29} clusters during synthesis. $t = 0$ is just before $NaBH_4$ addition. (a) UV−vis absorption spectra. (b) Maximum emission intensity over time. Inset: Normalized emission spectra at the beginning and end of the synthesis.

The observed changes in optical properties are consistent with earlier reports of the synthesis of Ag clusters capped with LA or LA functionalized with poly(ethylene glycol).[21,25,26] The synthesis process also appears similar to that of $Ag_{44}(SR)_{30}^{4-}$.[39] It is not, however, a general process that occurs for all Ag clusters; $Ag_{30}(SR)_{18}$ does not show a broad absorption feature during synthesis but instead a steady increase in absorbance of all its characteristic absorption features.[41]

Mass Spectrometry Study of Ag_{29} Clusters during Synthesis. Mass spectra of the Ag clusters during synthesis were recorded by taking aliquots which were purified with 1-butanol (BuOH). The purification is required to remove excess ligands and salts from the solution which interfere with the measurement. See Figure S1 for the effect of purification on the mass spectrum. Purification took 5−10 min, after which the sample was measured for around 15 min to collect sufficient scans. Mass spectra are shown in Figure 3. The clusters are observed as $[Ag_{29}(LA)_{12}^{3-} - (y + x)H^+ + xNa^+]^{(3+y)-}$, in overall charge states $(3 + y)- = 3-$, 4−, and 5−. Thus, multiple ion signals are observed in each charge state due to the association with Na^+ ions.

Our mass spectrometry data confirm the results of optical spectroscopy, namely that the Ag_{29} cluster appears early in the synthesis and that its concentration (signal/noise ratio) increases with time. For a number of the spectra (140, 208, and 298 min), the intensities of Na^+ adducts appear to show a bidisperse distribution and additional species are present. These are particularly evident in the $z = 4-$ overall charge state around m/z 1500. We believe this to be an effect of a slightly higher Na^+ concentration, either in the final purified aliquot or at some stage during the purification, which results in cluster degradation. A mass spectrum of purified clusters with added NaCl showed similarly bidisperse distributions, as well as the additional ion signals (see Figure S3).

A number of other cluster species were also observed, with sizes close to the main cluster: $Ag_{29}(LA)_{11}^{2-}$, $Ag_{28}(LA)_{11}^{2-}$, and some $Ag_{26}(LA)_{10}^{2-}$, shown in more detail in Figure S4. Interestingly, these were also observed in the mass spectrum of regenerated clusters,[19] where it was proposed that they were formed during the purification process. The ion signals of these clusters become less prominent as the synthesis progresses. A number of other ion signals are also observed but these increased in intensity during one measurement, suggesting degradation inside the capillary needle. Therefore, they are not analyzed further. These degradation products are marked with a red asterisk in Figure 3. We find no small cluster species such as $Ag_5(LA)_3^-$ or $Ag_6(LA)_3$ that were previously observed upon fragmentation of $Ag_{29}(LA)_{12}^{3-}$ during tandem MS or when applying a high sample cone voltage.[19] These small species

DOI: 10.1021/acs.jpcc.8b09360
J. Phys. Chem. C 2018, 122, 28351−28361

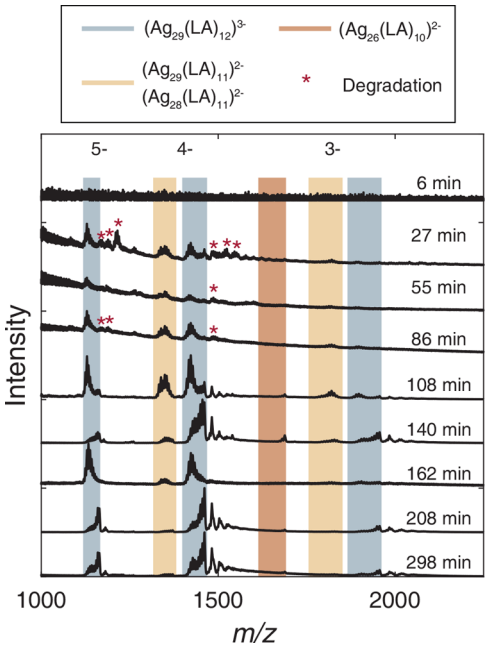

Figure 3. Mass spectra of Ag clusters at various times after $NaBH_4$ addition. The ion signals of $Ag_{29}(LA)_{12}^{3-}$ are marked in blue; those of the other observed clusters in red and yellow. Charges in the legend are the cluster core charges (on Ag and S atoms). The overall charge state, which includes deprotonation, is given above the 6 min spectrum. Deprotonation and subsequent association with Na^+ gives multiple signals for each cluster in each charge state. Ion signals marked with a red asterisk are found to increase in intensity during the mass spectrometry measurement, indicating they are formed by degradation due to light, heat, or high voltage. The given time is when the aliquot was taken.

evidently do not play an important role during the synthesis. Nor do we observe any ion signals at higher m/z values, although the source pressure of the mass spectrometer was kept to a minimum, which limits the ionization of larger species. Full mass spectra during synthesis can be found in Figure S2, along with a brief discussion of ion signals with low m/z.

It appears that the first initial burst of nucleation results in the formation of species that are not observed in our mass spectra. Within 30 min these are then converted to a mixture of Ag_{26}, Ag_{28}, and Ag_{29}, and over time size focusing makes the distribution more and more monodisperse. The initial species may be unobserved due to its high m/z or because it does not survive the purification protocol. The BuOH purification method was seen to have some influence on the synthesis. Around 6 h after the start of the synthesis, when the reservoir solution was bright reddish orange, the purified aliquots were held under a UV-lamp to check for luminescence. The first four aliquots (taken between 0 and 86 min) were brown and nonluminescent. Aliquot 5 was lighter in color and showed weak luminescence, while aliquots 6−9 were orange and strongly luminescent. This indicates that purification in the first 1−2 h removed species that are necessary for a good reaction (for example $NaBH_4$, or an excess of free LA). After 2 h the composition of the sample is such that complete purification will still yield clusters.

Mass spectrometry studies during synthesis of noble metal clusters are rare due to the challenging nature of such experiments. However, some studies have been done on $Au_{25}(SR)_{18}^-$. These indicate that the exact reaction pathway depends on synthesis conditions. An early study was of Au_{25} in tetrahydrofuran with phenylethanethiol as ligand and $NaBH_4$ as reducing agent.[42] It was found that the initial rapid nucleation and growth stage yielded a number of different cluster sizes up to Au_{102}. Magic sizes (Au_{25}, Au_{38} and Au_{102}) where noticeably present. Over the course of several days, the larger sizes where gradually converted to Au_{25}. A second study was done of aqueous Au_{25} clusters at high pH, capped with 3-mercaptobenzoic acid and using CO as a reducing agent.[43] Two growth stages were identified. The first stage involved reduction of the Au(I)-thiolate intermediate to give a narrow size distribution of clusters. In the second stage, size focusing converted these clusters into the thermodynamically most stable cluster; Au_{25}. The main difference with the study using $NaBH_4$ lies in the cluster sizes present after the first stage. For the clusters reduced with CO, these were significantly smaller, with fewer than 25 Au atoms. CO is a much slower, milder reducing agent than $NaBH_4$. It appears to be a general trend that mild reducing agents yield smaller initial species.[16] As our Ag_{29} clusters are prepared with $NaBH_4$, it is not unlikely that the first stage of the synthesis involves rapid reduction and growth to larger nanocluster cores, much as in the case of Au_{25} with $NaBH_4$.

EXAFS of Ag_{29} Clusters and during Synthesis. To confirm that the synthesis of Ag_{29} involves larger nanoparticles, we performed X-ray absorption spectroscopy. X-ray spectroscopy is element selective and does not require sample purification to remove excess ligands or salts. This makes it an ideal tool to investigate the synthesis of Ag_{29} clusters in further detail. As a first step, we characterized the as-synthesized Ag_{29} clusters with EXAFS to determine average coordination numbers and bond lengths. The cluster solution was concentrated (ca. 5×) using 3 kDa molecular mass cutoff filters to increase the signal-to-noise ratio and ensure accurate analysis. The clusters remain on the filter, while the filtrate is colorless. Previous work on Ag_{29} has demonstrated that the cluster solution contains no small Ag cluster species that may be removed with these filters.[19]

EXAFS data were fitted to one Ag−S and one Ag−Ag scattering path. A typical fit is shown in Figure 4, with the results of the fit in Table 1. The Ag−Ag coordination number was found to vary slightly depending on the fitting software and on the compound used to calculate the scattering paths and to some extent also which site was taken as the absorber for Ag_{29} with BDT. Typical values of the Ag−Ag coordination

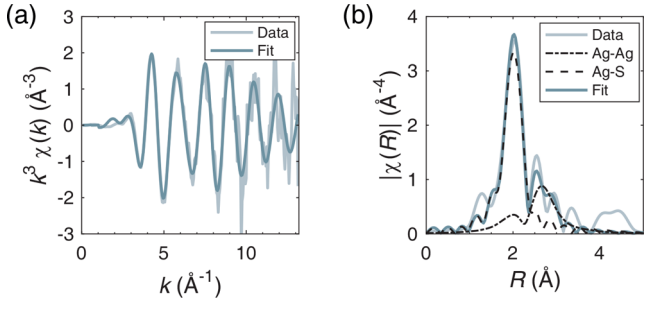

Figure 4. EXAFS of Ag cluster solution in (a) k and (b) R-space. The fit was done using scattering paths from Ag metal and Ag_2S. The contributions of each path are also shown in (b). The results of the fit are given in Table 1.

DOI: 10.1021/acs.jpcc.8b09360
J. Phys. Chem. C 2018, 122, 28351−28361

Table 1. Structural Parameters of Ag Clusters from EXAFS Analysis[a]

parameter	Ag−S	Ag−Ag
CN	1.26 ± 0.18	3.18 ± 1.41
R (Å)	2.47 ± 0.01	2.82 ± 0.05
σ^2 (10^{-3} Å^2)	4.16 ± 1.5	24.0 ± 7.9
E_0 (eV)	4.1 ± 1.7	1.4 ± 2.6

[a]CN is the coordination number, R the bond length, σ^2 the Debye-Waller factor, and E_0 the energy shift. The fit is shown in Figure 4. For this fit, R-factor = 0.020 and reduced χ^2 = 58. The amplitude reduction factor is not taken into account (i.e, $S_0^2 = 1$) for the values in the table.

number are between 2 and 5. The Ag−S does not change as much. Using two Ag−Ag scattering paths (one long and one short) did not improve the fit significantly (see Figure S6), and we therefore focus on EXAFS with one Ag−Ag scattering path. One average Ag−Ag bond length is also necessary for the analysis of EXAFS during synthesis, which will be discussed later.

The low Ag−Ag coordination number indicates a small particle size of perhaps several tens of atoms.[44,45] However, due to the presence of ligands an estimate that assumes a perfectly icosahedral or cuboctahedral shape will be inaccurate. The ubiquitous staple motif present in nanoclusters results in a significant fraction of metal atoms with bonds only to ligands, thus increasing the metal−ligand and lowering the metal−metal coordination numbers when compared to a perfectly icosahedral cluster with the same number of atoms.[46−48]

Our coordination numbers are similar to those found for $Au_{25}(SR)_{18}$.[47,48] Furthermore, the similarities in composition and optical properties between $Ag_{29}(LA)_{12}^{3-}$ and $Ag_{29}(BDT)_{12}(TPP)_4^{3-}$ (BDT, 1,3-benzenedithiol; TPP, triphenylphosphine) and the latter's known structure[31] allow a more direct comparison between our experimental results and the expected coordination numbers. $Ag_{29}(BDT)_{12}(TPP)_4^{3-}$ has an icosahedral Ag_{13} core surrounded by four Ag_3S_6 crowns, with the remaining four Ag atoms capped by TPP situated between these crowns. A schematic representation of this structure is shown in Figure S11. The shortest Ag−Ag bonds (up to 2.78 Å) are the 12 bonds from the central atom to those in the shell of the icosahedron. Next are the bonds between the atoms of the icosahedral shell, 12 bonds around 2.85 Å, 6 around 2.92 Å and a further 12 bonds of around 2.97 Å. Finally there are 24 long bonds of 3.05−3.16 Å that connect the Ag atoms in the crowns to each other and to the icosahedral surface. All in all, there are 42 bonds below 3.0 Å, which corresponds to an average Ag−Ag coordination number of 2.9, with average bond length of 2.87 Å. The distribution of Ag−S bond lengths shows a group of short and one of longer bonds. The 36 shorter bonds, below 2.5 Å, are those linking the Ag_3S_6 crowns to the icosahedral surface and most of the bonds within the crowns themselves. The longer Ag−S bonds are mainly those binding to the four external Ag atoms, which are capped by TPP ligands in the $Ag_{29}(BDT)_{12}(TPP)_4^{3-}$ cluster. Considering only the 36 shorter bonds, the average Ag−S coordination number is 2.5, with an average bond length of 2.47 Å.

These theoretical coordination numbers are in good agreement with our results. The Ag−S coordination number is perhaps slightly lower than expected. This may be due to a different surface structure of our Ag_{29} clusters compared to the $Ag_{29}(BDT)_{12}(TPP)_4^{3-}$, as our clusters do not have the additional TPP ligands. A small amount of cluster degradation/aggregation can also not be completely excluded as the cutoff filters are known to cause some cluster degradation.[19] However, UV−vis absorption spectra recorded before and after EXAFS show that radiation damage is limited (Figure S5). The experimental Ag−Ag and Ag−S bond lengths are in good agreement with expected values, and Debye−Waller factors are reasonably similar to those found for $Au_{25}(SR)_{18}$.[47]

To investigate the synthesis mechanism of Ag_{29} clusters, EXAFS was recorded of aliquots taken from the synthesis solution at various times after addition of $NaBH_4$. The aliquots were not purified or concentrated. Due to the low Ag concentration and limited time for measurements, spectra were recorded over a short k-range (up to k = 8.15 Å^{-1}) with low counts ($1-2 \times 10^4$ in the postedge). Calculated EXAFS of $Ag_{29}(LA)_{12}$ is shown in Figure S9 for the short k-range used here as well as the longer k-range used for previously synthesized Ag_{29} clusters. While the shorter k-range results in the loss of some detail, overall the features in R-space EXAFS are similar. To check for radiation damage, the aliquots were kept after EXAFS measurement. Around 9 h after addition of $NaBH_4$, when the synthesis was finished, all aliquots were found to luminescence red under a UV-lamp, showing that luminescent Ag_{29} clusters were formed despite exposure to X-rays.

All Fourier transformed EXAFS recorded during synthesis show two main peaks (Figure S8), corresponding to Ag−Ag and Ag−S scattering. To obtain good fits of EXAFS recorded during synthesis, we fixed Debye−Waller factors and bond lengths to the values of the as-synthesized cluster.[33] Additional fits were done using different constraints (only Debye−Waller factors or only bond lengths fixed). Coordination numbers obtained by all of the different fits are summarized in Figure 5, as box plots that show the median and the spread of the fit parameters. An alternative representation showing each obtained parameter as a separate data point is given in Figure S7. The EXAFS spectra themselves are presented in Figure S8. The first spectra are similar to calculated EXAFS of Ag in the

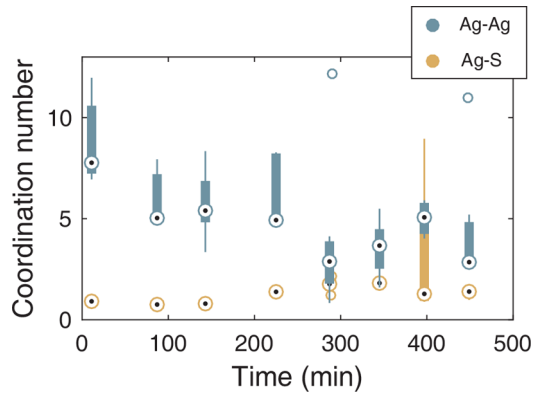

Figure 5. Ag−Ag and Ag−S coordination numbers during the synthesis of Ag_{29} clusters, shown as box plots. A number of fits were done for each spectrum, using different constraints, different software, or scattering paths calculated from different materials. The times are the start of each EXAFS measurement, measured from the addition of $NaBH_4$ to the synthesis mixture. The median is marked with a black dot. Box edges mark the 1st and 3rd quartiles, and whiskers extend to all data points within 1.5× the interquartile range. Values outside this range are plotted as outliers.

DOI: 10.1021/acs.jpcc.8b09360
J. Phys. Chem. C 2018, 122, 28351−28361

center and icosahedral sites of the cluster, with high Ag−Ag and low Ag−S coordination numbers; see Figure S9. Later in the synthesis, there is an increased resemblance to calculated EXAFS of Ag on the surface of the cluster (shell sites, see Figure S11) where there are more Ag−S bonds.

The general trend is clear: the Ag−Ag coordination number decreases over time while the Ag−S coordination number is fairly constant, with perhaps a slight increase. After 5 h, the coordination numbers are similar to those found for the as-synthesized sample, with little change during the rest of the synthesis. The initial high Ag−Ag coordination number is similar to that of $Au_{144}(SR)_{60}$ (Au−Au coordination number 7.2)[47] and so consistent with a particle of a hundred to a few hundred atoms. That monodisperse Ag_{29} is formed from such large species indicates that no other larger Ag cluster has a similar stability under the reductive synthesis conditions. In the size focusing process from $Ag_{\sim 100}$ to Ag_{29} many medium-sized clusters may be formed but none have sufficient stability to be present in the final solution. Neither are any medium-sized clusters observed in ESI-MS.

XANES of Ag_{29} Clusters. The Ag_{29} clusters were further studied by recording L_3-edge X-ray absorption spectra, focusing on the near-edge structure. The cluster solution was measured as a liquid jet in a chamber with He-atmosphere to avoid attenuation of X-rays in air. Due to the slight overpressure, the solution was saturated with He which prevented radiation damage (see Figure S10). Ag L_3-edge X-ray absorption spectra of freshly prepared Ag_{29} clusters in solution are shown in Figure 6, together with spectra of reference compounds Ag powder, Ag_2S, $AgNO_3$, and silver diethyldithiocarbamate (Ag(I)-thio). A spectrum of $AgNO_3$ in aqueous solution (10 mM) is shown in Figure S12 and has similar spectral features as that of solid $AgNO_3$.

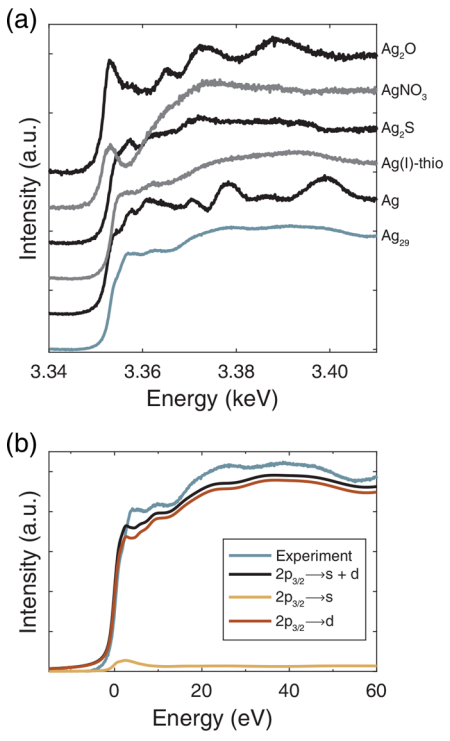

Figure 6. (a) XANES of Ag_{29} clusters together with spectra of reference compounds. (b) FDMNES calculations of Ag_{29}, using the dipole selection rules $\Delta l = \pm 1$ (s+d final states), $\Delta l = +1$ (d final states), and $\Delta l = -1$ (s final states).

In L_3-edge XAS, transitions from $2p_{3/2}$ to predominantly s- and d-states are observed, according to the dipole selection rule. In silver, the 2p → 5s transition is weaker by 1 order of magnitude than the 2p → 4d transition, thus the latter will dominate.[49] The first peak in the spectrum is called the whiteline, and for 4d metals its intensity is related to the number of empty 4d states.[50] Metallic silver has electron configuration $4d^{10}5s^1$, while ionic Ag^+ compounds also have a $4d^{10}$ state with no d-holes. Nevertheless, strong whitelines are observed, notably in $AgNO_3$ and Ag_2O. It has been found that the strong whiteline transition in these compounds is due to s−d hybridization, which results in $4d^{10-\delta}5s^{\delta}$ states. Hybridization becomes stronger with increased covalency of the Ag-ligand bond.[51] This is different from the general interpretation of whiteline intensities due to electron-withdrawal by ligands which would create $4d^95s^0$ states, i.e., Ag^{2+}. For bulk Ag, the features up to around 20 eV above the edge were assigned to pd states, while weak features close to the edge were due to excitations to 5s.[52]

The spectrum of Ag_{29} clusters shows two features just above the edge (3.358 and 3.363 keV), in addition to a shoulder on the edge, and some weak, broad features far above the edge. There are significantly fewer and weaker features than for Ag metal, as expected for clusters with a small number of atoms and lack of long-range order.[53] The spectrum of Ag_{29} resembles somewhat that of the Ag(I)-thio and Ag_2S, in particular the former. The structure of Ag(I)-thio has been shown to consist of bridged hexameric units $[AgS_2CN(C_2H_5)_2]_6$ where each Ag atom is connected to either 1 Ag and 4 S or 2 Ag and 3 S.[54] It is thus not unreasonable to compare this to the surface atoms of the Ag clusters. We further observe that the strong whiteline of $AgNO_3$ does not appear in the Ag_{29} spectrum. The shoulder on the rising edge of the Ag_{29} spectrum, which is also present in reference spectra of Ag metal and Ag_2S, is ∼1 eV higher in energy than the $AgNO_3$ whiteline. Furthermore, linear combination fits of the Ag_{29} spectrum to reference spectra did not reveal any contribution from $AgNO_3$. Clearly, this precursor is not present in the solution at any significant concentration. All in all, the observed spectral features of Ag_{29} are in accordance with (i) the small size of Ag_{29}, (ii) capping by thiolate ligands, and (iii) absence of any $AgNO_3$ precursor in the cluster solution.

The spectral features of the Ag_{29} XANES spectrum could be reproduced with high accuracy with FDMNES calculations, as seen in Figure 6, while calculations using FEFF (Figure S11) do not reproduce the two features above the edge. FEFF uses the muffin-tin approximation, where potentials are assumed to be spherically symmetrical. This approximation may break down for anisotropic systems, while for FDMNES the potential is allowed to take any shape.[55] Further information about the nature of the transitions in the spectrum can be obtained from FDMNES calculations using different selection rules. The default is the dipole selection rule $\Delta l = \pm 1$, i.e., from $2p_{3/2}$ to d and to s final states. Calculations were done considering $l \rightarrow l + 1$ and $l \rightarrow l - 1$ transitions separately. As can be seen, most spectral features can be assigned to $2p_{3/2} \rightarrow$ d transitions. However, the whiteline intensity is partially due to a transition to 5s. The spectra of four representative sites in Ag_{29} were also calculated separately, see Figure S11, and show that the

DOI: 10.1021/acs.jpcc.8b09360
J. Phys. Chem. C 2018, 122, 28351−28361

experimental spectrum in particular resembles the calculated spectra of surface sites, where Ag binds to both Ag and S.

XANES during the Synthesis of Ag_{29}. We attempted to record XANES of the Ag_{29} clusters synthesis in situ using the liquid jet setup. However, the synthesis was unsuccessful despite several attempts. The sample color turned from light yellow to black upon addition of $NaBH_4$ to the LA + $AgNO_3$ solution, with a broad absorption feature around 470 nm, but then did not change any further. It appears the initial nucleation and growth stage occurs similarly to when the synthesis is done in the lab, but the later size focusing stage of the reaction is hindered. The liquid jet setup differs from the standard reaction setup in a number of ways, most notably the exposure to X-rays and saturation of the synthesis solution with He, which may interfere with the required conditions for size focusing. This is discussed in more detail later.

Nevertheless, despite difficulties in performing the synthesis, we were able to record XANES of the solution at different stages during synthesis. If the synthesis was started in the lab and the solution transferred to the liquid jet setup after a certain amount of time, the synthesis stopped at this stage (there were no changes in the UV−vis absorption spectrum for several hours). XANES could then be recorded of this synthesis solution. By repeating this for a number of different waiting times, we could record XANES at various stages during synthesis. These spectra are shown in Figure 7. Note that even under laboratory conditions there is some variation in the synthesis time. Therefore, the times given in Figure 7 are approximate.

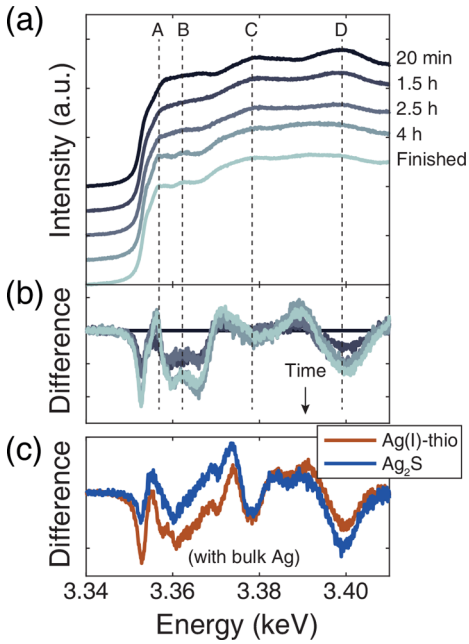

Figure 7. (a) XANES of Ag_{29} clusters at various stages of the synthesis. (b) The difference between each XANES spectrum and the "20 min" spectrum. Characteristic features are marked using dashed vertical lines. The given times indicate approximate progress of the synthesis from the moment of $NaBH_4$ addition. The first sample was prepared directly in the liquid jet setup, the second and third were kept in the lab until characteristic absorption features began to appear, and the fourth sample was kept in the lab until it was turning orange. (c) The difference between XANES of Ag(I)−thio and Ag_2S with bulk Ag.

A number of observations can be made from the spectra. First, the edge features reminiscent of Ag(I)−thio are not present early in the synthesis. Second, the features far above the edge around 3.38 and 3.40 keV become broader and less prominent over time. Weak, broad postedge features are commonly associated with smaller particles due to lack of long-range order, as observed in various studies including L_3-edge XANES of Au nanoparticles during synthesis,[56−58] L_3-edge XANES of Ag nanoparticles of various sizes,[53] and L_3-edge XANES of Au nanoparticles, either ligand-capped[59] or supported on oxides.[60] The difference spectra shown in Figure 7 are similar to difference spectra between Ag(I)−thio and bulk Ag or between Ag_2S and bulk Ag. XANES thus shows a decrease in particle size over time during the synthesis. The results agree very well with those of EXAFS and optical spectroscopy.

The spectra during synthesis were fitted to the spectrum of the previously prepared, finished clusters and that of the initial large species (first and last spectra in Figure 7). Results of the fits are given in Table 2 and show around 50−70% of Ag is present as Ag_{29} in the synthesis solution when characteristic UV−vis absorption features begin to appear.

Table 2. Fractions of Previously Prepared Ag_{29} Clusters ("Finished") and Large Ag Species Present Early in the Synthesis Synthesis ("20 min"), As Obtained by Linear Combination Fitting of XANES Spectra

spectrum	fraction "20 min"	fraction "finished"	*R* factor
1.5 h	0.53	0.47	0.00079
2.5 h	0.32	0.68	0.00039
4 h	0.13	0.87	0.00160

The very first stage of the synthesis is not observed with XANES (nor with EXAFS). In this stage, $AgNO_3$ is reduced and rapid nucleation and growth occur to give the large Ag nanoparticles. This occurs within 10 min of addition of the reducing agent and probably also to some extent before. The synthesis intermediate solution (LA + $AgNO_3$) already contains some $NaBH_4$ that was used to make LA water-soluble. Some Ag_{29} clusters will form in this solution even without further addition of $NaBH_4$.

Importance of Oxygen during Size Focusing. We propose that the synthesis cannot proceed without a small amount of oxygen and that it is the saturation of the solution with He rather than exposure to X-rays which prevents successful synthesis in the liquid jet setup used for XANES. When the synthesis was performed in the setup with He but without exposure to X-rays, Ag_{29} clusters were not formed. The UV−vis absorption spectrum only showed the broad absorption feature of the larger species and the characteristic features of the Ag_{29} clusters did not appear. In laboratory setting (without He) it was observed, though not systematically studied, that opening the vial briefly a few times during synthesis increased the rate of size focusing and led to faster appearance of the bright orange color and characteristic absorption features. In addition, when a small aliquot was transferred to a larger vial (containing more air) shortly after reduction with $NaBH_4$, it turned orange and luminescent faster than the parent sample.

It has been shown that oxygen plays an important role in etching to obtain monodisperse Au clusters. Au_{25} clusters can be prepared in tetrahydrofuran with tetra-*n*-octylammonium bromide, a phase transfer agent, provided there is some oxygen

DOI: 10.1021/acs.jpcc.8b09360
J. Phys. Chem. C 2018, 122, 28351−28361

present.[61] Etching of larger nanoparticles to clusters with excess thiols was similarly only observed when oxygen was present.[62] It was proposed that the synthesis of Au_{25} proceeds via larger, polydisperse nanoparticles that are etched with excess thiols. Thiols can react with oxygen to give thiyl radicals ($RS^{\bullet}$) which homolytically cleave Au−S bonds of the nanoparticles, resulting in $Au^{\bullet}$ species which were experimentally observed with electron paramagnetic resonance (EPR) spectroscopy.[62] The overall proposed mechanism for etching results in a layer-by-layer stripping of Au from the nanoparticle, until magic size clusters are obtained. Under inert atmosphere, no Au_{25} was obtained unless also radical initiators were added, confirming the importance of the diradical nature of oxygen. Similar observations were made for aqueous Au clusters, where in the absence of oxygen or radical initiators larger nanoparticles were formed instead of atomically monodisperse Au_{25} or Au_{102}.[63] Clearly, the role of oxygen in size focusing is of great importance both in organic and in aqueous solutions. For phosphine-capped Au clusters, it has likewise been shown that etching plays an important role in determining the final cluster size and may be controlled by the extent of ligand oxidation.[64,65]

To the best of our knowledge, no similar studies have been performed on Ag clusters, although a method involving multiple reduction and oxidation steps has been shown to obtain a stable cluster of unknown composition.[66] Another study found highly luminescent Ag could be formed after the reduction of a decomposed and initially polydisperse cluster sample.[67] In both these cases multiple reduction steps are used and size focusing does not yield the desired product by direct aging after the initial reduction.

The etching mechanism proposed for Au clusters involves both oxygen (or radical initiator) and excess thiols. If a similar mechanism is responsible for the etching to Ag_{29}, it is clear why clusters prepared with low LA concentrations[19] show weak luminescence and less pronounced absorption features when compared to the standard clusters; there is less ligand available for etching.

CONCLUSIONS

The synthesis process of $Ag_{29}(LA)_{12}^{3-}$ clusters was investigated to provide information on the mechanism. Optical spectroscopy, mass spectrometry, and X-ray spectroscopy were used to study the formation of the clusters. Upon addition of $NaBH_4$ to the synthesis intermediate solution of LA with $AgNO_3$, rapid nucleation and growth occurs resulting in the formation of Ag particles with a few hundred atoms. How these nanoparticles are formed is still unknown, as none of the techniques were able to observe the nucleation process. The reduction of $AgNO_3$ and subsequent nucleation are rapid enough that no $AgNO_3$ is observed with X-ray spectroscopy at any stage during the synthesis. From the polydisperse mixture of larger species, Ag_{29} clusters are formed and their concentration increases steadily over time. The etching process to obtain Ag_{29} requires oxygen and cannot proceed in inert atmosphere. Clusters with composition $Ag_{29}(LA)_{11}^{2-}$, $Ag_{28}(LA)_{11}^{2-}$, and $Ag_{26}(LA)_{10}^{2-}$ are observed in mass spectrometry during synthesis and may be intermediates in this process. No heavier cluster species are observed, proving that Ag_{29} is by far the most stable species in the range Ag_{29} to $Ag_{\sim 100}$ under the synthesis conditions.

ASSOCIATED CONTENT

Supporting Information

The Supporting Information is available free of charge on the ACS Publications website at DOI: 10.1021/acs.jpcc.8b09360.

Detailed protocols for synthesis and sample purification, additional mass spectra, UV−vis spectra before and after EXAFS, EXAFS fits and calculations, and additional XANES calculations (PDF)

AUTHOR INFORMATION

Corresponding Author

*E-mail: F.M.F.deGroot@uu.nl. Phone: +31 6 22736343.

ORCID

Marte van der Linden: 0000-0002-4085-0320
Pieter Glatzel: 0000-0001-6532-8144
Frank M. F. de Groot: 0000-0002-1340-2186

Notes

The authors declare no competing financial interest.

ACKNOWLEDGMENTS

The authors thank Hebatalla Elnaggar, Ties Haarman, Boyang Liu, and Ru-Pan Wang for their help during the beamtimes and Arjan Barendregt for help with mass spectrometry measurements. The ESRF and NWO are thanked for providing beamtime (proposals CH4969 and 26-01-1044). This work was financially supported by the Debye Graduate Programme (NWO project 022.004.016) and ESRF Graduate Programme; the mass spectrometry research was performed within the framework of NWO and supported by the large scale proteomics facility Proteins@Work (project 184.032.201) embedded in The Netherlands Proteomics Centre.

REFERENCES

(1) Lu, Y.; Chen, W. Sub-Nanometre Sized Metal Clusters: From Synthetic Challenges to the Unique Property Discoveries. *Chem. Soc. Rev.* **2012**, *41*, 3594−3623.

(2) Mathew, A.; Pradeep, T. Noble Metal Clusters: Applications in Energy, Environment, and Biology. *Part. Part. Syst. Charact.* **2014**, *31*, 1017−1053.

(3) Desireddy, A.; Conn, B. E.; Guo, J.; Yoon, B.; Barnett, R. N.; Monahan, B. M.; Kirschbaum, K.; Griffith, W. P.; Whetten, R. L.; Landman, U.; et al. Ultrastable Silver Nanoparticles. *Nature* **2013**, *501*, 399−402.

(4) Yang, H.; Wang, Y.; Huang, H.; Gell, L.; Lehtovaara, L.; Malola, S.; Häkkinen, H.; Zheng, N. All-Thiol-Stabilized Ag_{44} and $Au_{12}Ag_{32}$ Nanoparticles with Single-Crystal Structures. *Nat. Commun.* **2013**, *4*, 2422.

(5) AbdulHalim, L. G.; Ashraf, S.; Katsiev, K.; Kirmani, A. R.; Kothalawala, N.; Anjum, D. H.; Abbas, S.; Amassian, A.; Stellacci, F.; Dass, A.; et al. A Scalable Synthesis of Highly Stable and Water Dispersible $Ag_{44}(SR)_{30}$ Nanoclusters. *J. Mater. Chem. A* **2013**, *1*, 10148−10154.

(6) Yuan, X.; Zhang, B.; Luo, Z.; Yao, Q.; Leong, D. T.; Yan, N.; Xie, J. Balancing the Rate of Cluster Growth and Etching for Gram-Scale Synthesis of Thiolate-Protected Au_{25} Nanoclusters with Atomic Precision. *Angew. Chem., Int. Ed.* **2014**, *53*, 4623−4627.

(7) Wu, Z.; Suhan, J.; Jin, R. One-Pot Synthesis of Atomically Monodisperse, Thiol-Functionalized Au_{25} Nanoclusters. *J. Mater. Chem.* **2009**, *19*, 622−626.

(8) Negishi, Y.; Nobusada, K.; Tsukuda, T. Glutathione-Protected Gold Clusters Revisited: Bridging the Gap between Gold(I)-Thiolate Complexes and Thiolate-Protected Gold Nanocrystals. *J. Am. Chem. Soc.* **2005**, *127*, 5261−5270.

DOI: 10.1021/acs.jpcc.8b09360
J. Phys. Chem. C 2018, 122, 28351−28361

(9) Yu, Y.; Chen, X.; Yao, Q.; Yu, Y.; Yan, N.; Xie, J. Scalable and Precise Synthesis of Thiolated Au_{10-12}, Au_{15}, Au_{18}, and Au_{25} Nanoclusters via pH Controlled CO Reduction. *Chem. Mater.* **2013**, *25*, 946−952.
(10) Zhu, M.; Lanni, E.; Garg, N.; Bier, M. E.; Jin, R. Kinetically Controlled, High-Yield Synthesis of Au_{25} Clusters. *J. Am. Chem. Soc.* **2008**, *130*, 1138−1139.
(11) Qian, H.; Zhu, Y.; Jin, R. Size-Focusing Synthesis, Optical and Electrochemical Properties of Monodisperse $Au_{38}(SC_2H_4Ph)_{24}$ Nanoclusters. *ACS Nano* **2009**, *3*, 3795−3803.
(12) Qian, H.; Jin, R. Ambient Synthesis of $Au_{144}(SR)_{60}$ Nanoclusters in Methanol. *Chem. Mater.* **2011**, *23*, 2209−2217.
(13) Liu, C.; Li, G.; Pang, G.; Jin, R. Toward Understanding the Growth Mechanism of $Au_n(SR)_m$ Nanoclusters: Effect of Solvent on Cluster Size. *RSC Adv.* **2013**, *3*, 9778−9784.
(14) Zhu, M.; Qian, H.; Jin, R. Thiolate-Protected Au_{20} Clusters with a Large Energy Gap of 2.1 eV. *J. Am. Chem. Soc.* **2009**, *131*, 7220−7221.
(15) Meng, X.; Liu, Z.; Zhu, M.; Jin, R. Controlled Reduction for Size Selective Synthesis of Thiolate-Protected Gold Nanoclusters Au_n (n = 20, 24, 39, 40). *Nanoscale Res. Lett.* **2012**, *7*, 277.
(16) Wu, Z.; MacDonald, M. A.; Chen, J.; Zhang, P.; Jin, R. Kinetic Control and Thermodynamic Selection in the Synthesis of Atomically Precise Gold Nanoclusters. *J. Am. Chem. Soc.* **2011**, *133*, 9670−9673.
(17) Jin, R.; Qian, H.; Wu, Z.; Zhu, Y.; Zhu, M.; Mohanty, A.; Garg, N. Size Focusing: A Methodology for Synthesizing Atomically Precise Gold Nanoclusters. *J. Phys. Chem. Lett.* **2010**, *1*, 2903−2910.
(18) Yu, Y.; Yao, Q.; Luo, Z.; Yuan, X.; Lee, J. Y.; Xie, J. Precursor Engineering and Controlled Conversion for the Synthesis of Monodisperse Thiolate-Protected Metal Nanoclusters. *Nanoscale* **2013**, *5*, 4606−4620.
(19) van der Linden, M.; Barendregt, A.; van Bunningen, A. J.; Chin, P. T. K.; Thies-Weesie, D. M.; de Groot, F. M. F.; Meijerink, A. Characterisation, Degradation and Regeneration of Luminescent Ag_{29} Clusters in Solution. *Nanoscale* **2016**, *8*, 19901−19909.
(20) Walter, M.; Akola, J.; Lopez-Acevedo, O.; Jadzinsky, P. D.; Calero, G.; Ackerson, C. J.; Whetten, R. L.; Grönbeck, H.; Häkkinen, H. A Unified View of Ligand-Protected Gold Clusters as Superatom Complexes. *Proc. Natl. Acad. Sci. U. S. A.* **2008**, *105*, 9157−9162.
(21) Muhammed, M. A. H.; Aldeek, F.; Palui, G.; Trapiella-Alfonso, L.; Mattoussi, H. Growth of In Situ Functionalized Luminescent Silver Nanoclusters by Direct Reduction and Size Focusing. *ACS Nano* **2012**, *6*, 8950−8961.
(22) Newville, M. Fundamentals of XAFS. *Rev. Mineral. Geochem.* **2014**, *78*, 33−74.
(23) Penner-Hahn, J. E. In *Comprehensive Coordination Chemistry II*, 2nd ed.; McCleverty, J. A., Meyer, T. J., Eds.; Elsevier: Amsterdam, 2003; pp 159−186.
(24) Zhang, P. X-ray Spectroscopy of Gold-Thiolate Nanoclusters. *J. Phys. Chem. C* **2014**, *118*, 25291−25299.
(25) Adhikari, B.; Banerjee, A. Facile Synthesis of Water-Soluble Fluorescent Silver Nanoclusters and Hg(II) Sensing. *Chem. Mater.* **2010**, *22*, 4364−4371.
(26) Chin, P. T. K.; van der Linden, M.; van Harten, E. J.; Barendregt, A.; Rood, M. T. M.; Koster, A. J.; van Leeuwen, F. W. B.; de Mello Donega, C.; Heck, A. J. R.; Meijerink, A. Enhanced Luminescence of Ag Nanoclusters via Surface Modification. *Nanotechnology* **2013**, *24*, 075703.
(27) Nikitenko, S.; Beale, A. M.; van der Eerden, A. M. J.; Jacques, S. D. M.; Leynaud, O.; O'Brien, M. G.; Detollenaere, D.; Kaptein, R.; Weckhuysen, B. M.; Bras, W. Implementation of a Combined SAXS/WAXS/QEXAFS Set-Up for Time-Resolved In Situ Experiments. *J. Synchrotron Radiat.* **2008**, *15*, 632−640.
(28) Klementev, K. V. Extraction of the Fine Structure from X-ray Absorption Spectra. *J. Phys. D: Appl. Phys.* **2001**, *34*, 209−217.
(29) Ravel, B.; Newville, M. ATHENA, ARTEMIS, HEPHAESTUS: Data Analysis for X-ray Absorption Spectroscopy Using IFEFFIT. *J. Synchrotron Radiat.* **2005**, *12*, 537−541.
(30) Inorganic Crystal Structure Database. https://icsd.fiz-karlsruhe.de/.
(31) AbdulHalim, L. G.; Bootharaju, M. S.; Tang, Q.; Del Gobbo, S.; AbdulHalim, R. G.; Eddaoudi, M.; Jiang, D.-e.; Bakr, O. M. $Ag_{29}(BDT)_{12}(TPP)_4$: A Tetravalent Nanocluster. *J. Am. Chem. Soc.* **2015**, *137*, 11970−11975.
(32) Hanwell, M. D.; Curtis, D. E.; Lonie, D. C.; Vandermeersch, T.; Zurek, E.; Hutchison, G. R. Avogadro: An Advanced Semantic Chemical Editor, Visualization, and Analysis Platform. *J. Cheminf.* **2012**, *4*, 17.
(33) Korhonen, S. T.; Beale, A. M.; Newton, M. A.; Weckhuysen, B. M. New Insights into the Active Surface Species of Silver Alumina Catalysts in the Selective Catalytic Reduction of NO. *J. Phys. Chem. C* **2011**, *115*, 885−896.
(34) Bunău, O.; Joly, Y. Self-Consistent Aspects of X-ray Absorption Calculations. *J. Phys.: Condens. Matter* **2009**, *21*, 345501.
(35) Amestoy, P. R.; Guermouche, A.; L'Excellent, J. Y.; Pralet, S. Hybrid Scheduling for the Parallel Solution of Linear Systems. *Parallel Comput.* **2006**, *32*, 136−156.
(36) Guda, S. A.; Guda, A. A.; Soldatov, M. A.; Lomachenko, K. A.; Bugaev, A. L.; Lamberti, C.; Gawelda, W.; Bressler, C.; Smolentsev, G.; Soldatov, A. V.; et al. Optimized Finite Difference Method for the Full-Potential XANES Simulations: Application to Molecular Adsorption Geometries in MOFs and Metal-Ligand Intersystem Crossing Transients. *J. Chem. Theory Comput.* **2015**, *11*, 4512−4521.
(37) Rehr, J. J.; Kas, J. J.; Vila, F. D.; Prange, M. P.; Jorissen, K. Parameter-Free Calculations of X-ray Spectra with FEFF9. *Phys. Chem. Chem. Phys.* **2010**, *12*, 5503−5513.
(38) Wilcoxon, J. P.; Martin, J. E.; Provencio, P. Optical Properties of Gold and Silver Nanoclusters Investigated by Liquid Chromatography. *J. Chem. Phys.* **2001**, *115*, 998−1008.
(39) Bakr, O. M.; Amendola, V.; Aikens, C. M.; Wenseleers, W.; Li, R.; Dal Negro, L.; Schatz, G. C.; Stellacci, F. Silver Nanoparticles with Broad Multiband Linear Optical Absorption. *Angew. Chem., Int. Ed.* **2009**, *48*, 5921−5926.
(40) Chakraborty, I.; Erusappan, J.; Govindarajan, A.; Sugi, K. S.; Udayabhaskararao, T.; Ghosh, A.; Pradeep, T. Emergence of Metallicity in Silver Clusters in the 150 Atom Regime: A Study of Differently Sized Silver Clusters. *Nanoscale* **2014**, *6*, 8024−8031.
(41) Xia, N.; Yang, J.; Wu, Z. Fast, High-Yield Synthesis of Amphiphilic Ag Nanoclusters and the Sensing of Hg^{2+} in Environmental Samples. *Nanoscale* **2015**, *7*, 10013−10020.
(42) Dharmaratne, A. C.; Krick, T.; Dass, A. Nanocluster Size Evolution Studied by Mass Spectrometry in Room Temperature $Au_{25}(SR)_{18}$ Synthesis. *J. Am. Chem. Soc.* **2009**, *131*, 13604−13605.
(43) Luo, Z.; Nachammai, V.; Zhang, B.; Yan, N.; Leong, D. T.; Jiang, D.-e.; Xie, J. Toward Understanding the Growth Mechanism: Tracing all Stable Intermediate Species from Reduction of Au(I)-Thiolate Complexes to Evolution of Au_{25} Nanoclusters. *J. Am. Chem. Soc.* **2014**, *136*, 10577−10580.
(44) Jentys, A. Estimation of Mean Size and Shape of Small Metal Particles by EXAFS. *Phys. Chem. Chem. Phys.* **1999**, *1*, 4059−4063.
(45) Benfield, R. E. Mean Coordination Numbers and the Non-metal-Metal Transition in Clusters. *J. Chem. Soc., Faraday Trans.* **1992**, *88*, 1107−1110.
(46) Simms, G. A.; Padmos, J. D.; Zhang, P. Structural and Electronic Properties of Protein/Thiolate-Protected Gold Nanocluster with "Staple" Motif: A XAS, L-DOS, and XPS Study. *J. Chem. Phys.* **2009**, *131*, 214703.
(47) Yamazoe, S.; Takano, S.; Kurashige, W.; Yokoyama, T.; Nitta, K.; Negishi, Y.; Tsukuda, T. Hierarchy of Bond Stiffnesses within Icosahedral-Based Gold Clusters Protected by Thiolates. *Nat. Commun.* **2016**, *7*, 10414.
(48) MacDonald, M. A.; Chevrier, D. M.; Zhang, P.; Qian, H.; Jin, R. The Structure and Bonding of $Au_{25}(SR)_{18}$ Nanoclusters from EXAFS: the Interplay of Metallic and Molecular Behavior. *J. Phys. Chem. C* **2011**, *115*, 15282−15287.

DOI: 10.1021/acs.jpcc.8b09360
J. Phys. Chem. C 2018, 122, 28351−28361

(49) Šipr, O.; Rocca, F.; Dalba, G. Real-Space Multiple-Scattering Analysis of Ag L_1- and L_3-edge XANES Spectra of Ag_2O. *J. Synchrotron Radiat.* **1999**, *6*, 770−772.
(50) Pearson, D. H.; Ahn, C. C.; Fultz, B. White Lines and d-electron Occupancies for the 3d and 4d Transition Metals. *Phys. Rev. B: Condens. Matter Mater. Phys.* **1993**, *47*, 8471−8478.
(51) Miyamoto, T.; Niimi, H.; Kitajima, Y.; Naito, T.; Asakura, K. Ag L_3-edge X-ray Absorption Near-Edge Structure of $4d^{10}$ (Ag^+) Compounds: Origin of the Edge Peak and its Chemical Relevance. *J. Phys. Chem. A* **2010**, *114*, 4093−4098.
(52) Sham, T. K. L-edge X-ray-Absorption Systematics of the Noble Metals Rh, Pd, and Ag and the Main-Group Metals In and Sn: A Study of the Unoccupied Density of States in 4d Elements. *Phys. Rev. B: Condens. Matter Mater. Phys.* **1985**, *31*, 1888−1902.
(53) Padmos, J. D.; Zhang, P. Surface Structure of Organosulfur Stabilized Silver Nanoparticles Studied with X-ray Absorption Spectroscopy. *J. Phys. Chem. C* **2012**, *116*, 23094−23101.
(54) Yamaguchi, H.; Kido, A.; Uechi, T.; Yasukouchi, K. The Crystal and Molecular Structure of Silver(I) N,N-Diethyldithiocarbamate. *Bull. Chem. Soc. Jpn.* **1976**, *49*, 1271−1276.
(55) Joly, Y. X-ray Absorption Near-Edge Structure Calculations Beyond the Muffin-Tin Approximation. *Phys. Rev. B: Condens. Matter Mater. Phys.* **2001**, *63*, 125120.
(56) Ohyama, J.; Teramura, K.; Higuchi, Y.; Shishido, T.; Hitomi, Y.; Aoki, K.; Funabiki, T.; Kodera, M.; Kato, K.; Tanida, H.; et al. An In Situ Quick XAFS Spectroscopy Study on the Formation Mechanism of Small Gold Nanoparticles Supported by Porphyrin-Cored Tetradentate Passivants. *Phys. Chem. Chem. Phys.* **2011**, *13*, 11128−11135.
(57) Ohyama, J.; Teramura, K.; Higuchi, Y.; Shishido, T.; Hitomi, Y.; Kato, K.; Tanida, H.; Uruga, T.; Tanaka, T. In Situ Observation of Nucleation and Growth Process of Gold Nanoparticles by Quick XAFS Spectroscopy. *ChemPhysChem* **2011**, *12*, 127−131.
(58) Ohyama, J.; Teramura, K.; Shishido, T.; Hitomi, Y.; Kato, K.; Tanida, H.; Uruga, T.; Tanaka, T. In Situ Au L_3 and L_2 Edge XANES Spectral Analysis During Growth of Thiol Protected Gold Nanoparticles for the Study on Particle Size Dependent Electronic Properties. *Chem. Phys. Lett.* **2011**, *507*, 105−110.
(59) Yiu, Y. M.; Zhang, P.; Sham, T. K. The Electronic Properties and L_3 XANES of Au and Nano-Au. *Technical Proceedings of the 2003 Nanotechnology Conference and Trade Show* **2003**, *3*, 183−186.
(60) van Bokhoven, J. A.; Miller, J. T. d Electron Density and Reactivity of the d Band As a Function of Particle Size in Supported Gold Catalysts. *J. Phys. Chem. C* **2007**, *111*, 9245−9249.
(61) Parker, J. F.; Weaver, J. E. F.; McCallum, F.; Fields-Zinna, C. A.; Murray, R. W. Synthesis of Monodisperse $[Oct_4N^+][Au_{25}(SR)_{18}^-]$ Nanoparticles, with Some Mechanistic Observations. *Langmuir* **2010**, *26*, 13650−13654.
(62) Dreier, T. A.; Ackerson, C. J. Radicals Are Required for Thiol Etching of Gold Particles. *Angew. Chem.* **2015**, *127*, 9381−9384.
(63) Dreier, T. A.; Compel, W. S.; Wong, O. A.; Ackerson, C. J. Oxygen's Role in Aqueous Gold Cluster Synthesis. *J. Phys. Chem. C* **2016**, *120*, 28288−28294.
(64) Ligare, M. R.; Johnson, G. E.; Laskin, J. Observing the Real Time Formation of Phosphine-Ligated Gold Clusters by Electrospray Ionization Mass Spectrometry. *Phys. Chem. Chem. Phys.* **2017**, *19*, 17187−17198.
(65) Pettibone, J. M.; Hudgens, J. W. Gold Cluster Formation with Phosphine Ligands: Etching as a Size-Selective Synthetic Pathway for Small Clusters? *ACS Nano* **2011**, *5*, 2989−3002.
(66) Cathcart, N.; Mistry, P.; Makra, C.; Pietrobon, B.; Coombs, N.; Jelokhani-Niaraki, M.; Kitaev, V. Chiral Thiol-Stabilized Silver Nanoclusters with Well-Resolved Optical Transitions Synthesized by a Facile Etching Procedure in Aqueous Solutions. *Langmuir* **2009**, *25*, 5840−5846.
(67) Yuan, X.; Setyawati, M. I.; Tan, A. S.; Ong, C. N.; Leong, D. T.; Xie, J. Highly Luminescent Silver Nanoclusters with Tunable Emissions: Cyclic Reduction−Decomposition Synthesis and Antimicrobial Properties. *NPG Asia Mater.* **2013**, *5*, e39.

DOI: 10.1021/acs.jpcc.8b09360
J. Phys. Chem. C 2018, 122, 28351−28361